Converter Control Impacts on Efficacy of Protection Relays in HVDC-Connected Offshore Wind Farms

Gao, Guoqing; Wu, Heng; Wang, Xiongfei

Published in:
2022 IEEE 13th International Symposium on Power Electronics for Distributed Generation Systems, PEDG 2022

DOI (link to publication from Publisher):
10.1109/PEDG54999.2022.9923236

Publication date:
2022

Document Version
Accepted author manuscript, peer reviewed version

Converter Control Impacts on Efficacy of Protection Relays in HVDC-Connected Offshore Wind Farms

Guoqing Gao, Heng Wu, Xiongfei Wang
AAU Energy, Aalborg University, Aalborg, Denmark
gga@energy.aau.dk, hew@energy.aau.dk, xwa@energy.aau.dk

***Abstract*— The high-voltage dc (HVDC)-connected offshore wind farms (OWF) is a power electronic converter dominated power system, where conventional protections, including overcurrent protection, distance protection, and differential protection, may not operable effectively. To reveal the impact of converter control on the efficacy of conventional protection relays, this paper first investigates the highly controlled fault current characteristics of HVDC system and OWF. Then, the basic operation principles of conventional protection relays are presented to elaborate their responses to the fault currents of HVDC system and of OWF, based on which, scenarios that lead to the malfunction of protection relays are identified. Finally, the theoretical analysis is verified by electromagnetic transient (EMT) simulations.**

Keywords—Offshore wind farms, converter control, protection relay, power electronic converter, fault current

I. INTRODUCTION

Nowadays offshore wind farms (OWFs) are increasingly deployed in the power grid and connected through the high-voltage dc (HVDC) transmission systems. The OWF-HVDC system is based on power electronic converters, which features high controllability and operational flexibility [1]. The fault currents of OWF and HVDC system are highly dependent on their control strategies, which can significantly differ from that of synchronous generators (SGs). This difference poses challenges to reliable operations of conventional protection relays which are designed based on fault currents of SGs.

The fault currents of SGs are dependent on the electromagnetic dynamics of electrical machines, which can be treated as an equivalent impedance behind a voltage source. Therefore, the fault current characteristics of SGs can be summarized as the following aspects:

1) The magnitude of fault current is of high (≥ 3 p.u.) magnitude.
2) The fault current is highly inductive [2].
3) Significant negative- and zero-sequence current can be provided for unbalanced faults.

Different from SGs, the fault current responses of converters are highly dependent on their control strategies, which features:

1) A low magnitude (≤ 1.5 p.u.) fault current, which is generally dependent on the thermal limit of power semiconductor devices.
2) The phase angle of fault current is highly controllable and usually mandated by the grid code. Besides, it is also affected by the manufacturer specific and the proprietary control system [3].
3) The zero-sequence current of grid-connected converters is commonly suppressed. The injection of negative-sequence current is not commonly required, with the exception of German grid code [4].

The commonly used protection methods of power grids include overcurrent protection, distance protection, current differential protection, etc. There have been research works reported on interactions between inverter-based resources and protection systems. In [5], the performance of overcurrent relays (OCRs) used with the centralized photovoltaic (PV) system is investigated. It is reported that OCRs on the PV inverters may not be effective due to the limited fault current of inverters. In contrast to inverters connected directly to ac grids, the fault current characteristics of OWF-HVDC system are much more complex, since the fault currents from both sides are controllable, and there is no grid code on the fault current injection of offshore HVDC converter station. In [6], [7], the efficacy of OCRs in OWF-HVDC system is investigated. Yet, it is assuemd that the phase angle of fault current contributed by each converter is the same when calculating the total fault current. The impact of fault-current phase angle difference of converters on the efficacy of OCRs is overlooked.

The efficacy of distance protection that are implemented in the transmission lines connecting SG and wind farm is evaluated in [8], [9]. Due to the presence of fault resistance, the impedance measured by distance protection relay contains additional terms introduced by the fault resistance and the ratio of fault currents. Since the phase angle of fault current from converters follows the grid code requirement, the ratio of fault currents between SG and converters is fixed, and then the distance protection can be revised to be susceptible to the additional impedance. However, for the HVDC-OWF system, the phase angle of fault current of HVDC system, especially the modular multilevel converter (MMC)-HVDC system, can be controlled to an arbitrary value, due to the lack of specific

This work is funded by the European Union's Horizon 2020 Research and Innovation Program under the Marie Sklodowska-Curie grant agreement No 861398.

978-1-6654-6618-9/22/$31.00 ©2022 European Union

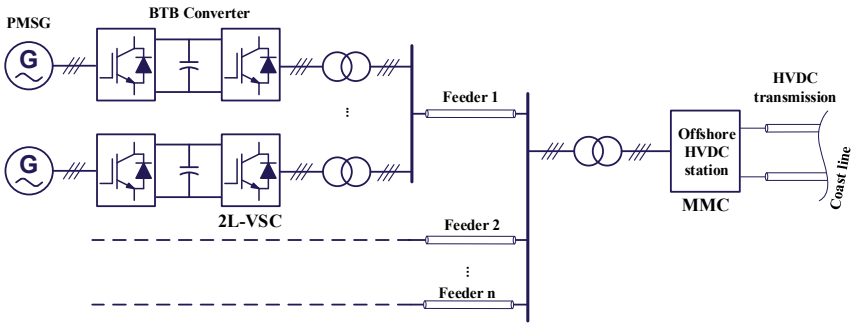

Fig. 1: System diagram of the HVDC-Connected Offshore Wind Farms

requirement. Consequently, revising the distance protection according to the expected impedance is not applicable.

The performance of current differential protection (CDP) is discussed in PV power plants [10], where the ratio of differential current over the restraint current is derived, considering the effect of control system parameters and grid voltage imbalance coefficient. It is found that the differential protection can operate reliably when the grid is strong. The performance of CDP implemented in the ac transmission line connected WF is evaluated in [11]. It is demonstrated that the CDP is immune to the phase angle difference of the fault currents from wind farm and infinite bus. This phenomenon is because the magnitude of fault current from the infinite bus outweighs that of the wind farm. In the OWF-HVDC system, both sides of the transmission line are fed by converters, where the phase angle difference of fault currents from both sides of the OWF and HVDC system can lead to a failure of the differential protection.

This paper performs a systematic study on the impacts of converter control on the efficacy of overcurrent, distance, and differential relays in OWF-HVDC system. The system structure and the characteristics of the controlled fault current from converters are elaborated first. Then, the impact of controlled fault current on conventional protection relays is discussed. Finally, the mechanisms of protection-relay failures are revealed and validated through the electromagnetic transient (EMT) simulation.

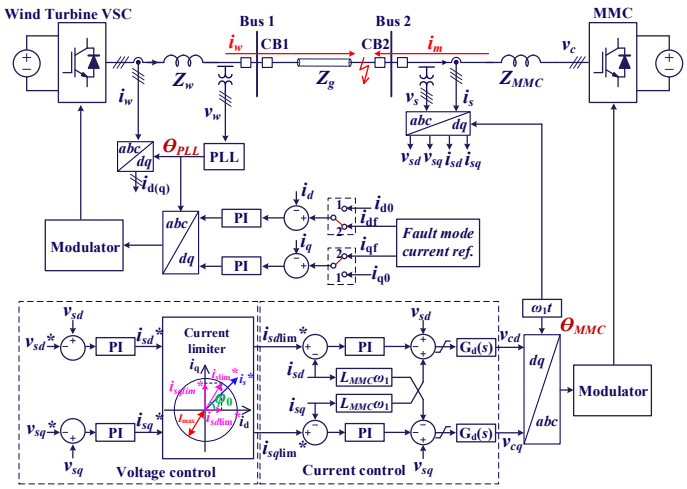

Fig. 2: Schematic of the HVDC-connected offshore wind farms

II. System Description

The system diagram of HVDC-OWF is illustrated in Fig. 1. The offshore AC grid is a converters-dominated system, where the grid-side voltage-source converters (VSCs) of wind turbines are connected, through submarine cables, to the MMC-HVDC station. MMC adopts the grid-forming (GFM) control to provide the voltage and frequency reference for the offshore AC grid, while the grid-side VSCs of wind turbines can adopt the grid-following (GFL) control in this study.

The equivalent diagram of the HVDC-connected OWF is depicted in Fig. 2. For simplicity, the OWF is aggregated as a single GFL-VSC. In the event of a short-circuit fault, the output current reference of VSC is switched to the fault mode according to the fault ride-through requirement. The reactive current injection of VSC follows the grid code [12] as shown in Fig. 3, which is a tabulated function of the magnitude of the terminal voltage. Accordingly, the injected active current can be calculated as

$$\begin{aligned} |i_{\mathrm{df}}| &= \sqrt{I_{\mathrm{lim}}^2 - |i_{\mathrm{qf}}|^2} \\ \varphi_1 &= \arctan\left(\frac{i_{qf}}{i_{df}}\right) \end{aligned} \tag{1}$$

Therefore, the phase angle φ_1 of the fault current from VSC is dependent on the distribution of the active and

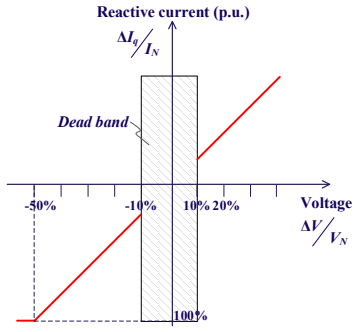

Fig. 3: The additional required reactive current during voltage

reactive current during fault. Further, the active current is aligned with the *d*-axis of the synchronous reference frame, which is oriented to the point of common coupling (PCC) voltage with a phase-locked loop (PLL). Hence, the phase angle φ_1 of the fault current is defined as the angle difference between the *d*-axis and the current vector.

The GFM control system of MMC consists of an outer voltage loop and an inner current loop. To avoid the overcurrent of MMC, the current limiter is inserted at the output of the outer-loop voltage controller. The phase angle of the terminal voltage of MMC equals to $\Theta_{\mathrm{MMC}}=\omega_1 t$.

After the inception of low-impedance short-circuit fault as shown in Fig. 2, the terminal voltage drop of MMC will lead to the magnitude increase of the fault current reference until the current limiter is activated, with which the magnitude of fault current from MMC is limited. The phase angle φ_0 of the fault current from MMC is defined as the angle difference between its *d*-axis and current vector. Since there is no grid code requirement on φ_0, it can be controlled to an arbitary value. As will be discussed in the following sections, the value of φ_0 has a significant impact on the efficacy of conventional protection relays.

III. Control Impacts on Efficacy of Protection Relays

A. Overcurrent Relays

Fig. 4 illustrates a general system diagram of an OWF, where four wind farm clusters are connected with the MMC. In the case of short-circuit fault on cable feeders, the fault current infeed from other converters will converge to the fault location, which addresses the concern that the fault current from a single converter is too small to trip the OCR. Therefore, the OCR is widely utilized in cable feeders connected to the collector bus of OWF [6]. OWF has bidirectional fault currents, the magnitude and phase angle of which are highly controlled by converters. The bidirectional fault currents infeed from the upstream and downstream networks could alter the magnitude and direction of the fault current flowing through the OCR. For instance, in the event of a low-impedance short circuit fault at point F_1 as shown in Fig. 4, the fault current infeed from MMC and other wind farm clusters will converge at OCR1. The trip time t_{OCR1} [7] can be expressed as (2), which is a function of the magnitude of $\dot{I}_{sum}$ in per unit.

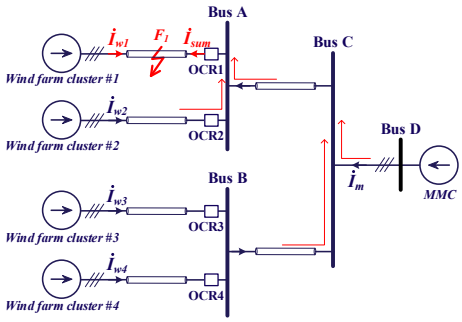

Fig. 4: Illustration of overcurrent protection in offshore wind farm with multiple fault current infeeds

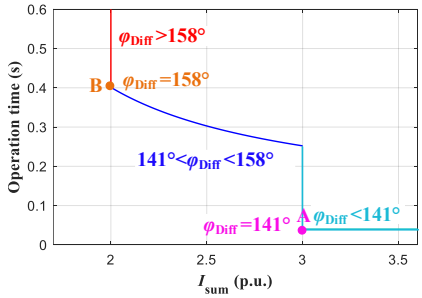

Fig. 5: The operation characteristics of OCR

$$t_{\mathrm{OCR1}}=\begin{cases}\infty, & \left|\dot{I}_{sum}\right|<2\ p.u.\\ \dfrac{0.14\times 0.04}{\left|\dot{I}_{sum}\right|^{0.02}-1}, & 2\ p.u.\le\left|\dot{I}_{sum}\right|<3\ p.u.\\ 0.04, & \left|\dot{I}_{sum}\right|\ge 3\ p.u.\end{cases} \tag{2}$$

Accordingly, the operation characteristics of the OCR is depicted in Fig. 5, where $\varphi_{\mathrm{diff}} = \varphi_0 - \varphi_1$ is the phase angle difference of the fault current from MMC and wind farm clusters. Besides, the capacity of MMC equals to the sum of that of the four identical wind farm clusters in this case. If φ_{diff} is greater than 158°, OCR1 fails to trip. As φ_{diff} decreases, the operation time of OCR1 gradually reduces to the definite time 0.04s. Since φ_1 is determined by the grid code as illustrated in Fig. 3, φ_{diff} is actually controlled by φ_0, which has significant impact on the operation and speed of OCR.

B. Distance Protection

The illustration of the distance protection in the OWF-HVDC system is shown in Fig. 6, where the distance protection relays are equipped on the wind farm side and MMC side, respectively. After fault inception, the calculated impedance by distance protection relay jumps to the short-circuit impedance [13] with a small magnitude and a large impedance angle. Therefore, the distance protection can easily distinguish between the normal and fault condition by properly setting the operating characteristic. If the calculated impedance is within the operating characteristic, the relay will be effectively tripped.

In the event of a symmetrical 3-phase-to-ground fault with a fault resistance R_{F}, the fault currents $\dot{I}_w$ and $\dot{I}_m$ are fully determined by the control of VSC and of MMC, which are different from the circuit-dependent fault current of SGs. The measured impedance by relay1 and relay2 can be expressed as:

$$Z_{\mathrm{relay1}} = aZ_{LF} + R_F + \frac{\dot{I}_m}{\dot{I}_w}R_F \tag{3}$$

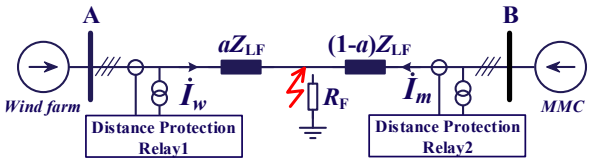

Fig. 6: Distance protection in converters dominated system

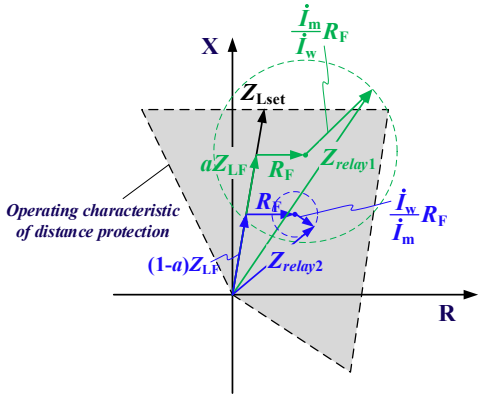

Fig. 7: Illustration of the operating characteristic of distance protection and the measured impedance

$$Z_{\text{relay2}} = (1-a)Z_{LF} + R_F + \frac{\dot{I}_w}{\dot{I}_m}R_F \tag{4}$$

Based on (3) and (4), the phasor diagram of Z_{relay1} and Z_{relay2} can be plotted, as shown in Fig. 7. It is known from the last terms of (3) and (4) that both Z_{relay1} and Z_{relay2} are affected by the ratio of $\dot{I}_m$ to $\dot{I}_w$, namely $\dot{I}_m / \dot{I}_w = \left|\dot{I}_m / \dot{I}_w\right| \angle\varphi_{diff}$.

In practice, there are usually multiple OWFs connected to one MMC-HVDC station. The capacity of MMC is n times ($n \geq 1$) of that of a single OWF. Therefore, the length of the vector representing $\left(\dot{I}_m / \dot{I}_w\right)R_F$ will be n^2 times of that representing $\left(\dot{I}_w / \dot{I}_m\right)R_F$. Besides, the direction of the vector representing $\left(\dot{I}_m / \dot{I}_w\right)R_F$ is determined by φ_{diff}, which is the phase angle difference of fault currents from both sides of the feeder, i.e., φ_0-φ_1. It is worth mentioning that φ_{diff} is also an arbitrary value as φ_0 can be freely selected based on the fault current contorl of MMC. In the case that the length of vector $\left(\dot{I}_m / \dot{I}_w\right)R_F$ is relatively large, it can be seen from Fig. 7 that the measured impedance Z_{relay1} on wind farm side could get beyond the operating characteristic of the distance protection if φ_{diff} is not properly controlled, with which the relay will fail to trip.

To verify the theoretical analysis, EMT simulations are carried out in the OWF-HVDC system with distance protection adopted. The trajectories of impedance measured by the distance protection at MMC side and wind farm side are shown in Fig. 8 considering the symmetrical 3-phase-to-ground fault. When the capacity of MMC equals to that of the wind farm ($R_{3\text{Ø-grd}}$=2Ω, φ_0=70°) as shown in Fig. 8(a), the trajectories of Z_{relay1} and Z_{relay2} are within the operating characteristic during transient. Therefore, the wind farm side Relay1 and MMC side Relay2 can both trip after fault inception. If the capacity ratio $S_{\text{MMC}}/S_{\text{windFarm}}$ increases to 1.5 as shown in Fig. 8(b), the trajectory of Z_{relay1} will cross the operating characteristic and the wind farm side Relay1 fails to trip, which validates the conclusion that the distance protection on wind farm side is prone to malfunction when the capacity of MMC increases. If the fault resistance $R_{3\text{Ø-grd}}$ decreases to 1.5Ω as shown in Fig. 8(c), the trajectory of Z_{relay1} is confined within the operating characteristic during transient and Relay1 can normally trip again. This is because that the

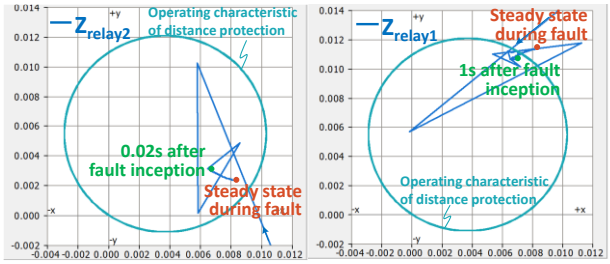

(a) $S_{MMC} = S_{WindFarm}$, $R_{3\text{Ø-}grd}$=2Ω (0.005 p.u.), φ_0=70°

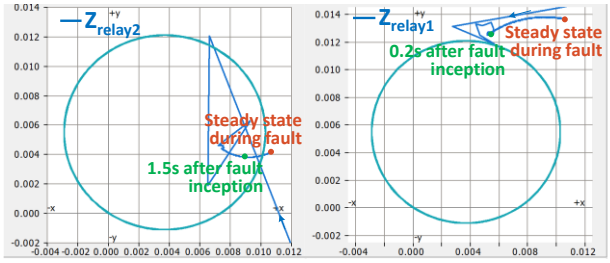

(b) S_{MMC} / $S_{WindFarm}$ =1.5, $R_{3\text{Ø-}grd}$=2Ω (0.005 p.u.), φ_0=70°

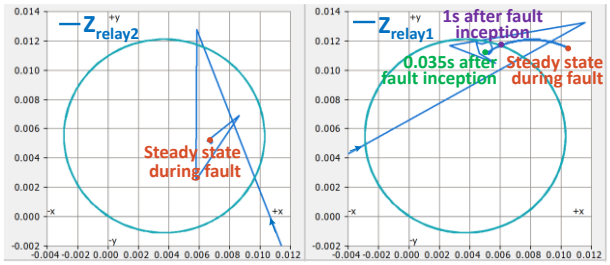

(c) S_{MMC} / $S_{WindFarm}$ =1.5, $R_{3\text{Ø-}grd}$=1.5Ω (0.0035 p.u.), φ_0=70°

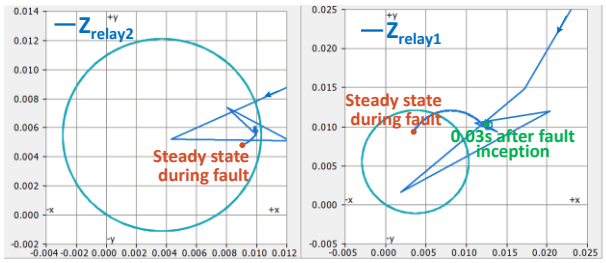

(d) S_{MMC} / $S_{WindFarm}$ =1.5, $R_{3\text{Ø-}grd}$=1.5Ω (0.0035 p.u.), φ_0=-20°

Fig. 8: Trajectories of impedance measured by the MMC side and wind farm side distance protection

reduced fault resistance will shorten the vectors representing R_F and $\left(\dot{I}_m / \dot{I}_w\right)R_F$ as shown in Fig. 7, restraining Z_{relay1} to cross the operating characteristic of distance protection. However, if the phase angle φ_0 of the fault current $\dot{I}_m$ decreases to -20°, Relay1 fails to trip as shown in Fig. 8(d). This is because the phase angle of fault current $\dot{I}_w$ will follow the grid code [12] after fault inception, and then the direction of the vector representing $\left(\dot{I}_m / \dot{I}_w\right)R_F$ is determined by the control of φ_0. The trajectory of Z_{relay1} during the transient will cross the operating characteristic if φ_0 is not properly controlled. Therefore, it can be concluded that the distance protection on the wind farm side is prone to malfunction, especially when the capacity of MMC increases and φ_{diff} is not properly controlled.

C. Current Differential Protection

The illustration of CDP when both sides are converters is shown in Fig. 9. The CDP measures the fault currents of both sides of the protected zone, i.e., $\dot{I}_w$ and $\dot{I}_m$, which are fully determined by the control of converters.

The criteria of CDP are shown in (5), where I_{diff} and I_{res} are differential current and restraint current, respectively. $I_{op[0]}$ is the threshold value to eliminate the effect of measurement error or the capacitive current of cables, etc. The coefficient k is the bias factor [14], which defines the slop of the operating characteristic and is typically set as 0.8 for feeder protection of OWF.

$$\begin{cases} I_{diff} \geq I_{op[0]}, \quad I_{diff} = \left|\dot{I}_w + \dot{I}_m\right| \\ I_{diff} \geq k \cdot I_{res}, I_{res} = \left|\dot{I}_w - \dot{I}_m\right| \end{cases} \tag{5}$$

The relationship between $\dot{I}_w$, $\dot{I}_m$, I_{diff}, and I_{res} with different capacity ratio and phase angle difference is illustrated in Fig. 11. If the capacity of MMC outweighs that of the wind farm as shown in Fig. 11(a), the phase angle difference φ_{diff} has minor impact on I_{diff} and I_{res}. Therefore, the relay of CDP can normally trip in this case corresponding to point *A* of Fig. 10. In contrast, if the wind farm and MMC have the similar capacity as shown in Fig. 11(b)(c), the phase angle difference φ_{diff} has significant impact on I_{diff} and I_{res}. In Fig. 11(b), φ_{diff} is greater than 90° and the relay fails to trip

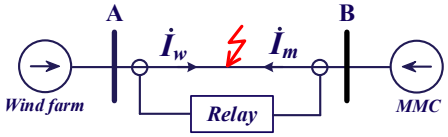

Fig. 9: CDP when both sides are converters

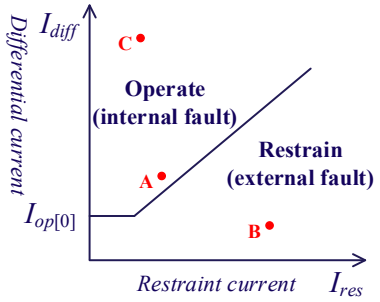

Fig. 10: Operating characteristic of CDP

corresponding to point *B* of Fig. 10. Besides, φ_{diff} is less than 90° in Fig. 11(c) and the relay can normally trip corresponding to point *C* of Fig. 10.

To validate the theoretical analysis above, simulation studies are carried out considering the 3-phase-to-ground fault ($R_{3\text{Ø-grd}}$=80Ω) with CDP adopted in OWF-HVDC system, and the results are given in Fig. 12. When the capacity of MMC is equal to that of the wind farm and the phase angle φ_0 of the fault current from MMC is 70°, the magnitude of restraint current is greater than that of the differential current and the trajectory of them is always below the relay operating characteristic as shown in Fig. 12(a). Thus, the relay of CDP fails to trip in this case. When φ_0 decreases to 10°, the transient trajectory of restraint and differential currents is above the relay operating characteristic, and hence the relay can successfully trip as shown in Fig. 12(b). If the capacity ratio further increases to 10 and φ_0 equals to 70°, the magnitude of restraint current is greater than that of the differential current until about 6 fundamental power cycles after fault inception as shown in Fig. 12(c). Although the relay can finally trip in this case, the response is very slow and takes around 130 ms. When φ_0 decreases to 10°, the magnitude of differential current is greater than that of the restraint current 3 ms after fault inception as shown in Fig. 12(d), and hence, the relay can quickly trip. According to the time-domain

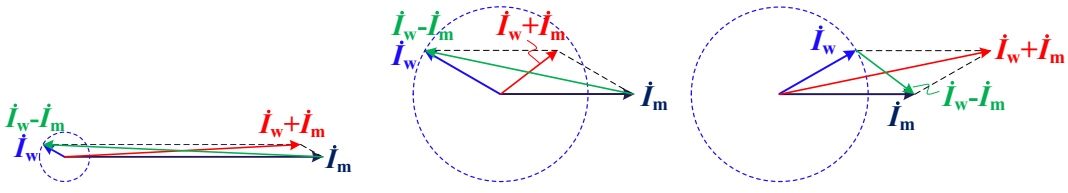

(a) S_{MMC} / $S_{WindFarm}$=10 (b) S_{MMC} / $S_{WindFarm}$=1.5, φ_{diff} > 90° (c) S_{MMC} / $S_{WindFarm}$=1.5, φ_{diff} < 90°

Fig. 11: The relationship between $\dot{I}_w$, $\dot{I}_m$, I_{diff}, and I_{res} with different capacity ratio and phase angle difference

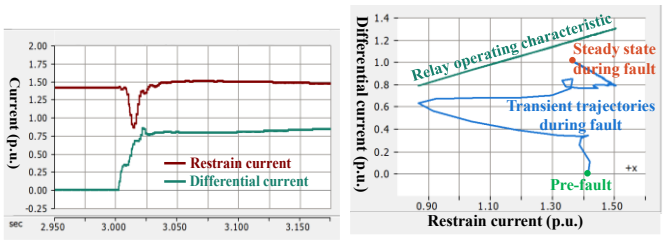

(a) $S_{MMC} = S_{WindFarm}$, φ_0=70° (relay fails to trip)

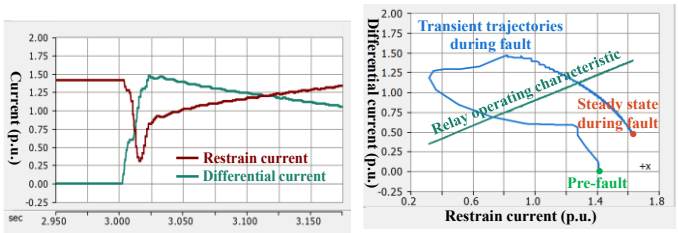

(b) $S_{MMC} = S_{WindFarm}$, φ_0=10° (relay trips)

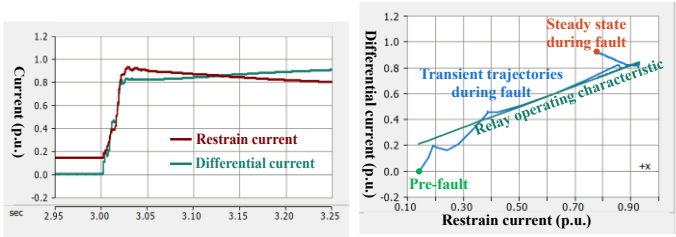

(c) S_{MMC} / $S_{WindFarm}$=10, φ_0=70° (Relay trips but is very slow)

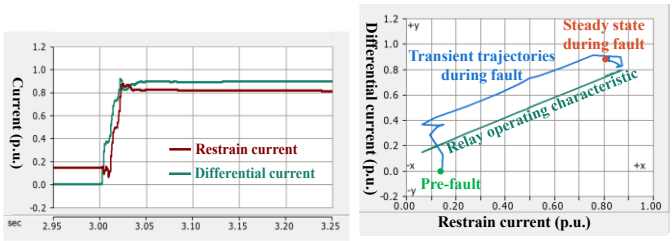

(d) S_{MMC} / $S_{WindFarm}$=10, φ_0=10° (relay trips)

Fig. 12: Time-domain waveforms and trajectory of differential and restrain currents

waveforms and the trajectories of differential and restraint currents, the comparison of the four simulation cases is shown in TABLE I. It is obvious that CDP is prone to malfunction when the capacity of wind farm increases, which is opposite to the characteristics of distance protection. Besides, the controlled phase angle of the fault current from MMC could lead to the slow response or even failure of CDP. Therefore, the phase angle control of the fault current from MMC can be coordinated with the conventional protections to improve their reliability and sensitivity.

TABLE I. CONCLUSION OF THE SIMULATION CASES

		Fault-current phase angle of MMC	
		70°	**10°**
Capacity ratio of MMC to VSCs	**1**	Relay fail to trip	Relay successfully trips (12 ms after fault inception)
	10	Relay trips (very slow: 130 ms after fault inception)	Relay successfully trips (fast: 3 ms after fault inception)

IV. CONCLUSION

This paper has discussed the converter-control impacts on the efficacy of conventional protection relays in HVDC-connected OWF. The control of VSC and MMC during fault conditions is demonstrated, which illustrates that the phase angle difference φ_{diff} between the fault currents of OWF and MMC can be an arbitrary value, due to the control flexibility of the MMC. Further analysis reveals that the improper setting of φ_{diff} can lead to the malfunction of the overcurrent protection, distance protection, and current differential protection under the different capacity ratios between MMC and OWF. Finally, the EMT simulation results are given to verify the theoretical analysis.

REFERENCES

[1] V. Yaramasu, B. Wu, P. C. Sen, S. Kouro, and M. Narimani, "High-power wind energy conversion systems: State-of-the-art and emerging technologies," *Proc. IEEE,* vol. 103, pp. 740-788, May 2015.

[2] Y. W. Li, D. M. Vilathgamuwa, P. C. Loh, and F. Blaabjerg, "A dual-functional medium voltage level DVR to limit downstream fault currents," *IEEE Trans. Power Electron.,* vol. 22, pp. 1330-1340, Jul. 2007.

[3] A. Korompili, Q. Wu, H. J. R. Zhao, and S. E. Reviews, "Review of VSC HVDC connection for offshore wind power integration," *Renew. Sustain. Energy Rev,* vol. 59, pp. 1405-1414, Jun. 2016.

[4] I. Erlich and U. Bachmann, "Grid code requirements concerning connection and operation of wind turbines in Germany," in *IEEE Power Energy Soc. Gen. Meet.*, 2005, vol. 2, pp. 1253-1257.

[5] K. Jia, C. Gu, Z. Xuan, L. Li, and Y. Lin, "Fault Characteristics Analysis and Line Protection Design Within a Large-Scale Photovoltaic Power Plant," *IEEE Trans. Smart Grid,* vol. 9, pp. 4099-4108, Jan. 2018.

[6] S. Chaudhary, "Control and Protection of Wind Power Plants with VSC-HVDC Connection," Ph.D. dissertation, Department of Energy Technology, Aalborg University, 2011.

[7] Y. Jing, "Control and operation of MMC-HVDC system for connecting offshore wind farm," Ph.D. dissertation, University of Strathclyde, 2019.

[8] A. Hooshyar, M. A. Azzouz, and E. F. El-Saadany, "Distance Protection of Lines Emanating From Full-Scale Converter-Interfaced Renewable Energy Power Plants—Part II: Solution Description and Evaluation," *IEEE Trans. Power Del.,* vol. 30, pp. 1781-1791, Nov. 2015.

[9] A. Hooshyar, M. A. Azzouz, and E. F. El-Saadany, "Distance Protection of Lines Emanating From Full-Scale Converter-Interfaced Renewable Energy Power Plants—Part I: Problem Statement," *IEEE Trans. Power Del.,* vol. 30, pp. 1770-1780, Nov. 2015.

[10] Y. Liang, W. Li, and G. Xu, "Performance Problem of Current Differential Protection of Lines Emanating from Photovoltaic Power Plants," *Sustainability,* vol. 12, Jan. 2020.

[11] Y. Li, K. Jia, T. Bi, R. Yan, W. Li, and B. Liu, "Analysis of line current differential protection considering inverter-interfaced renewable energy power plants," in *IEEE PES Innovative Smart Grid Technologies Conference Europe*, 2017, pp. 1-6.

[12] M. Graungaard Taul, X. Wang, P. Davari, and F. Blaabjerg, "Current Reference Generation Based on Next-Generation Grid Code Requirements of Grid-Tied Converters During Asymmetrical Faults," *IEEE Trans. Emerg. Sel. Topics Power Electron.,* vol. 8, pp. 3784-3797, Jul. 2020.

[13] G. Ziegler, *Numerical distance protection: principles and applications*. John Wiley & Sons, 2011.

[14] G. Ziegler, *Numerical differential protection: principles and applications*. John Wiley & Sons, 2012.